Gamma Ray Observations of a Giant Flare from the Magnetar SGR 1806−20

D. M. Palmer,[1] S. Barthelmy,[2] N. Gehrels,[2] R. M. Kippen,[1] T. Cayton,[1] C. Kouveliotou,[3] D. Eichler,[4] R. A. M. J. Wijers,[5] P. M. Woods,[6] J. Granot,[7] Y. E. Lyubarsky,[4] E. Ramirez-Ruiz,[8] L. Barbier,[2] M. Chester,[9] J. Cummings,[2,10] E. E. Fenimore,[1] M. H. Finger,[6] B. M. Gaensler,[11] D. Hullinger,[2] H. Krimm,[2,12] C. B. Markwardt,[2,13] J. A. Nousek,[9] A. Parsons,[2] S. Patel,[6] T. Sakamoto,[2,10] G. Sato,[14] M. Suzuki[15] and J. Tueller[2]

[1] Los Alamos National Laboratory, Los Alamos, NM, 87545, USA

[2] NASA/Goddard Space Flight Center, Greenbelt, MD, 20771, USA

[3] NASA/Marshall Space Flight Center, NSSTC, XD-12, 320 Sparkman Dr., Huntsville, AL 35805, USA

[4] Department of Physics, Ben Gurion University, POB 653, Beer Sheva 84105, Israel

[5] Astronomical Institute "Anton Pannekoek", University of Amsterdam, Kruislaan 403, 1098 SJ, Amsterdam, the Netherlands

[6] Universities Space Research Association, NSSTC, XD-12, 320 Sparkman Dr., Huntsville, AL 35805, USA

[7] Kavli Institute for Particle Astrophysics and Cosmology, Stanford University, P.O. Box 20450, MS 29, Stanford, CA 94309, USA

[8] Institute for Advanced Study, Einstein Drive, Princeton, NJ 08540, USA

[9] Pennsylvania State University, University Park, PA, 16802, USA

[10] National Research Council, 500 Fifth St. N.W. Washington, DC, 20001, USA

[11] Harvard-Smithsonian Center for Astrophysics, 60 Garden Street MS-6, Cambridge, MA 02138, USA

[12] Universities Space Research Association, Goddard Space Flight Center , Greenbelt, MD, 20771, USA

[13] University of Maryland, College Park, MD, 20742, USA

[14] Institute of Space and Astronautical Science (ISAS) / JAXA, 3-1-1 Yoshinodai, Sagamihara, Kanagawa 229-8510, Japan

[15] Saitama University, 55 Shimo-Okubo, Sakura-ku, Saitama City, Saitama 338-8570, Japan

Magnetars[1] comprise two classes of rotating neutron stars (Soft Gamma Repeaters (SGRs) and Anomalous X-ray Pulsars), whose X-ray emission is powered

by an ultrastrong magnetic field, $B \sim 10^{15}$ G. Occasionally SGRs enter into active episodes producing many short X-ray bursts; extremely rarely (about once per 50 years per source), SGRs emit a giant flare, an event with total energy at least 10^3 higher than their typical bursts.[2–4] Here we report that, on 2004 December 27, SGR 1806–20 emitted the brightest extra-solar transient event ever recorded, even surpassing the full moon brightness for 0.2 seconds. The total (isotropic) flare energy is 2×10^{46} erg, ∼100 times higher than the only two previous events, making this flare a once in a century event. This colossal energy release likely occurred during a catastrophic reconfiguration of the magnetar's magnetic field. Such an event would have resembled a short, hard Gamma Ray Burst (GRB) if it had occurred within 40 Mpc, suggesting that extragalactic SGR flares may indeed form a subclass of GRBs.

Only two other giant flares have previously been recorded, one each from SGR 0526–66 on 1979 March 5[2,3] and SGR 1900+14 on 1998 August 27.[4] Intense X-ray burst activity from SGR 1900+14 preceded the 1998 August 27 flare[5]; there are very few observations of SGR 0526–66 preceding the 1979 March 5 event. In the year leading up to the SGR 1806–20 flare, well-sampled X-ray monitoring observations of the source with the *Rossi X-ray Timing Explorer (RXTE)* indicated that it was also entering a very active phase,[6] emitting more frequent and intense bursts and showing enhanced persistent X-ray emission that was, indeed, a prelude to the unprecedented giant flare.

On 2004 December 27 the *Swift* satellite[7] was among a large number of spacecraft inundated by radiation from SGR 1806–20.[8,9,s3] The Burst Alert Telescope (BAT)[s4] is a γ-ray (15-350 keV) coded aperture imager on *Swift*. Although *Swift* was turned away from the SGR location, and so the event illuminated the detector from behind, the flux that passed through the spacecraft and shielding of the BAT provided excellent measurements of the event. The BAT light curve (Figure 1, and with more detail in the *supplementary figures*) demonstrates that magnetar giant flares are remarkably similar: all three start with an initial very short and spectrally hard main spike, followed by an extended softer tail highly modulated at the neutron star's spin period. The bright, main spike lasts ~ 0.5 s and is followed by a tail

with ~ 50 cycles of high-amplitude pulsations at the known rotation period of SGR 1806–20 (7.56 s). In the Dec. 27 event we also notice a 1-s long, flat-topped precursor burst at 142 s before the main spike.

Several astounding new properties of a magnetar flare are revealed from the superb time resolution of the BAT. Figure 1b plots the sharp initial rise of the main spike in time bins of 100μs, equivalent to the light crossing time of the neutron star diameter. Prior to the steep rise of the initial spike, the count rate was rising for 40 ms at a slower rate (shown in *supplementary figure* 2) and had reached roughly 30,000 cps (above a ~ 9 kcps background) by $t = 0$. At that point it increased by a factor of more than 100 in less than 1.5 ms (0.3 ms e-folding rise time). This is followed by at least one dip and continued brightening (additional dips would not be visible due to instrument saturation) on its way to the peak. The flare rise is thus resolved for the first time. The flux during the spike, though heavily attenuated, saturated the BAT modules, precluding a reliable flux measurement. We have used, therefore, the SOPA[s1] and ESP[s2] instruments located on geosynchronous satellites (see *Supplementary Methods* Section) to measure the main peak flux. The SOPA instruments are small silicon detectors designed with fast event processing to measure the high particle fluxes found in orbit. During the peak of the burst, each detector had a dead-time greater than 50%, but this level of saturation can be accurately corrected for. We fit the SOPA data with an exponential-cutoff power law (finding a characteristic temperature $kT = 0.48(4)$ MeV and a power-law photon index $-0.2(1)$) and derive a flux of $5.0(3)\,\mathrm{erg\,cm^{-2}\,s^{-1}}$ over an 0.160 s integration time for 45 keV to 10 MeV photons; the corresponding fluence is $0.80(5)\,\mathrm{erg\,cm^{-2}}$. This duration and spectral hardness is in the range of characteristics found for the short, hard subclass of classic GRBs.[14]

Since the count rate was significantly lower during the tail, we were able to model the off-axis illumination and calibrate the flux and spectroscopy measurements (see *Supplementary Methods*). We find the tail of the burst to have an energy fluence of $1.0(5) \times 10^{-3}\ \mathrm{erg\,cm^{-2}}$ at photon energies > 60 keV. The spectral fits are consistent with thermalized spectra with $kT \sim 15-30$ keV as seen in previous flares, implying a comparable energy fluence below our 60 keV threshold. Accounting for the $10-60$ keV photons, we project the total tail fluence to

be $\gtrsim 2 \times 10^{-3}\,\mathrm{erg\,cm^{-2}}$, roughly 0.3% that of the main peak. For a distance to SGR 1806–20 of $15d_{15}\,\mathrm{kpc}$,[15] we then find an (isotropic equivalent) energy release of $2 \times 10^{46}d_{15}^2\,\mathrm{erg}$ in the spike, and $5 \times 10^{43}d_{15}^2\,\mathrm{erg}$ in the tail. Thus, the isotropic equivalent energy in the initial spike is about two orders of magnitude larger than that in the other two giant flares, while the energy in the tail is comparable. Indeed, a radio afterglow[16] was detected from this flare with a luminosity 500 times that from the August 27 flare, suggesting a truly large difference in the prompt burst energy. The consistency of the tail energies among the three flares is attributable to the fact that they are limited by the storage capacity of the magnetic field[1,17] and should be as constant from source to source as the field energy. Thus, the tail luminosities, which are expected to be at roughly the magnetically modified Eddington limit, should also be similar, as observed. The extent of magnetic reconnection, on the other hand, governs the prompt energy release during the main spike; this can vary greatly from one event to the next, even within the same source.

The pulse profile in the tail of the flare just after the main spike features one large peak and two smaller adjacent local maxima separated by about 1/4 of a rotation cycle (Figure 2 and *supplementary figure* 1). The relative intensities of the peaks change during the tail, but their phases remain fixed, indicating that the field configuration does not change substantially during the tail and that the released energy comes from the trapped fireball.

The polar B−field of SGR 1806–20 has been calculated[18] from its spin-down rate to be $\sim 1.6 \times 10^{15}\,\mathrm{G}$, corresponding to a external magnetic field energy of $2 \times 10^{47}\,\mathrm{erg}$, which indicates that at most $10d_{15}^{-2}/f$ such giant flares can be produced from the star in its lifetime (here f is the beaming factor).

We used RXTE to measure the spin frequency and spin-down rate of the SGR 30 days after the flare.[19] The frequency is consistent with an extrapolation of the pre-flare frequency with pre- and post-flare spin-down rates. Thus, the December 27 flare could not have caused a rapid, lasting change in the spin frequency greater than $\sim 2 \times 10^{-5}$ Hz; this, despite the much larger apparent burst energy, limits the frequency change to be at most comparable to that seen following the August 27 flare.[20] The post-flare spin-down rate, $-3.15(9) \times 10^{-12} Hz\ s^{-1}$, although lower than it was shortly before the flare, is still in its historical range.

The three time scales in the phenomenon, a) the rise time of ~ 1 ms, b) the duration of the hard spike, ~ 0.5 s, and c) the duration of the tail, several minutes - are similar for all three giant flares. These are attributed to the Alfvén propagation times in a) the magnetosphere and b) the star, and c) the cooling time of the trapped pair fireball, respectively.[1,17]

Violent energy dissipation can occur anywhere in the magnetically dominated region, which includes the outer layers of the neutron star: if an energy of $10^{46}E_{46}$ erg is dissipated roughly uniformly in the reconnection region of volume $10^{18}V_{18}$ cm^3, then matter above the layer at density $1 \times 10^8 E_{46}/V_{18}$ g/cm^3 will have an energy density larger than its gravitational potential and become unbound. This is about 10^{24} g, which can be ejected into the magnetosphere at fractions of the speed of light. Such a mass ejection (which need not be isotropic) is enough to power the observed radio nebula and its 0.3c expansion.[16]

The two earlier flares would have been detectable by existing instruments only within ~ 8 Mpc, and, therefore, it was not previously thought that such flares could be the source of the short, hard GRBs. The main spike of the December 27 giant flare would have resembled a short, hard GRB had it occurred within 40 d_{15} Mpc, encompassing even the Virgo cluster. Magnetar formation rate is expected to follow the star formation rate, which is (for $z = 0$) 1.3 ± 0.2 M$_\odot$ yr^{-1} in our Galaxy[21] and $0.013^{+0.02}_{-0.007}$ M$_\odot$ Mpc^{-3} yr^{-1} averaged over intergalactic scales.[22] This suggests that the Burst And Transient Source Experiment (*BATSE*) onboard the Compton Gamma Ray Observatory would have triggered on such events as short GRBs at a rate of $N_{\mathrm{BATSE}} = 80(\dot{N}_{\mathrm{gal,GF}}/0.03$ yr$^{-1})d_{15}^3$ yr^{-1}, to be compared to an estimate of the 4πsr *BATSE* rate of about 150 yr^{-1}. Here, $\dot{N}_{\mathrm{gal,GF}}$ is the average rate of giant flares in the Galaxy similar to the Dec. 27 event. The observed isotropic distribution of short BATSE GRBs on the sky and the lack of excess events from the direction of the Virgo cluster suggests that only a small fraction ($\lesssim 0.05$) of these events can be SGR giant flares within $\lesssim 40$ Mpc. This implies either: $d \lesssim 7$ kpc; $N_{\mathrm{gal,GF}} \lesssim (3) \times 10^{-3}$ yr^{-1} on average for a Galaxy like our own; or the luminosity distribution includes even larger SGR flares that can be seen at a greater distance.[23] One possible distinction of these from the classic GRB population may well come from their radio observations, as their radio afterglows should not be detectable beyond ~ 1 Mpc. The fraction of SGR events among what are now classified as short GRBs

may not be predominant, but it should be detectable. This will be testable with future *Swift* observations.

1. Thompson, C. & Duncan, R. C. The soft gamma repeaters as very strongly magnetized neutron stars. I. Radiative mechanism for outbursts. *MNRAS* **275**, 255–300 (1995).

2. Mazets, E. P., Golenetskii, S. V., Ilinskii, V. N., Apetkar, R. L. & Guryan, Y. A. Observations of a flaring X-ray pulsar in Dorado. *Nature* **282**, 587–589 (1979).

3. Fenimore, E. E., Klebesadel, R. W., & Laros, J. G. The 1979 March 5 Gamma-Ray Transient: Was it a Classic Gamma-Ray Burst? *ApJ* **460**, 964–975, (1996).

4. Hurley, K., et al. A giant periodic flare from the soft gamma-ray repeater SGR 1900+14. *Nature* **397**, 41–43 (1999).

5. Hurley, K., Kouveliotou, C., Woods, P., Cline, T., Butterworth, P., Mazets, E., Golenetski, S. & Frederiks, D. Reactivation and Precise Interplanetary Network Localization of the Soft Gamma Repeater SGR 1900+14. *ApJ* **510**, L107–L109 (1999).

6. Woods, P. M., Kouveliotou, C., Göğüş, E., Patel, S., Hurley, K. & Swank, J. Gradual Brightening of SGR 1806-20. *ATEL* **313** (2004).

7. Gehrels, N., et al. The *SWIFT* Gamma-Ray Burst Mission. *ApJ* **611**, 1005–1020 (2004).

8. Borkowski, D., Gotz, D., Mereghetti, S., Mowlavi, N., Shaw, S., & Turler, M. Giant flare from SGR 1806-20 detected by INTEGRAL. *GCN* **2920** (2004).

9. Palmer, D. M., et al. SGR1806-20: Swift-BAT observation of the 041227 super-flare. *GCN* **2925** (2004).

10. Boggs, S., Hurley, K., Smith, D. M., Lin, R.P., Hurford, G., Hajdas, W., & Wigger, C. SGR 1806-20, RHESSI observations of the 041227 giant flare. *GCN* **2936** (2005).

11. Barthelmy, S.D. Burst Alert Telescope (BAT) on the Swift MIDEX mission. *SPIE* **5165**, 175–189 (2004).

12. Belian, R. D., Gisler, G. R., Cayton T., Christensen, R. High-Z energetic particles at geosynchronous orbit during the great solar proton event series of October 1989. *JGR* **97(A11))** 16,897–16,906 (1992).

13. Meier, M. M., Belian, R. D., Cayton, T. E., Christensen, R. A., Garcia, B., Grace, K. M., Ingraham, J. C., Laros, J. G., Reeves, G. D., The Energy Spectrometer for Particles (ESP): instrument description and orbital performance. in the proceedings of *Workshop on the Earth's Trapped Particle Environment*, AIP Conference proceedings **383** 203–210 (1996).

14. Kouveliotou,C., Meegan,C. A., Fishman,G. J., Bhat,N. P., Briggs,M. S., Koshut,T. M., Paciesas,W. S., & Pendleton,G. N. *ApJ* **413**, L101–L104 (1993).

15. Corbel, S. & Eikenberry, S. S. The connection between W31, SGR 1806–20, and LBV 1806–20: Distance, extinction, and structure. *A&A* **419**, 191–201 (2004).

16. Gaensler, B. M., et al. An Expanding Radio Nebula Produced by a Giant Flare from the Magnetar SGR 1806-20. *Nature* **accepted** (2005).

17. Thompson, C. & Duncan, R. C. The giant flare of 1998 August 27 from SGR 1900+14. II. Radiative mechanism and physical constraints on the source. *ApJ* **561**, 980–1005 (2001).

18. Woods, P. M., Kouveliotou, C., Göğüş, E., Finger, M. H., Swank, J., Markwardt, C. B., Hurley, K. & van der Klis, M. Large Torque Variations in Two Soft Gamma Repeaters. *ApJ* **576**, 381–390 (2002).

19. Woods, P. M., Kouveliotou, C., Göğüş, E., Finger, M., Patel, S., Swank, J. & Hurley, K Spin and Pulsed X-ray Flux Properties of SGR 1806-20 after the Giant Flare. *ATEL* **407** (2005).

20. Woods, P. M., Kouveliotou, C., van Paradijs, J., Finger, M. H., Thompson, C., Duncan, R. C., Hurley, K., Strohmayer, T., Swank, J. & Murakami, T. Variable Spin Down in the Soft Gamma Repeater SGR 1900+14 and Correlations with Burst Activity. *ApJ* **524**, L55–L58 (1999).

21. Kennicutt, R.C., Jr. The star formation law in galactic disks. *ApJ* **344**, 685–703 (1989).

22. Gallego, J., Zamorano, J., Aragon-Salamanca, A. & Rego, M. The Current Star Formation Rate of the Local Universe. *ApJ* **455**, L1 (1995).

23. Eichler, D. Waiting for the Big One: a new class of soft gamma-ray repeater outbursts? *MNRAS* **335**, 883–886 (2002).

24. Feroci, M., Hurley, K., Duncan, R.C. & Thompson, C. The Giant Flare of 1998 August 27 from SGR 1900+14 I. An Interpretive Study of *BeppoSAX* and *Ulysses* Observations. *ApJ* **549**, 1021–1038 (2001).

Correspondence should be addressed to palmer@lanl.gov

Supplementary Information accompanies the paper on www.nature.com/nature.

Supplementary Methods

SOPA and ESP peak fluence determination

Each Synchronous Orbit Particle Analyzer (SOPA[s1]) consists of three identical particle telescopes that function as ΔE–E particle spectrometers. Energy depositions in a 3000 μm thick, 0.25 cm^2 silicon E-sensor that occur without a finite ΔE signal are identified as electrons and pulse-height analyzed into 10 deposited energy channels. To provide accurate measurements of large particle fluxes, each SOPA telescope has a small field of view (11°) and fast readout electronics (5.5 μs deadtime). These characteristics also make the SOPA electron channels ideal for intense γ-ray fluxes that would overwhelm larger detectors designed for maximum sensitivity to weak signals. The 10 SOPA electron channels cover the deposited-energy range 45 keV to >1.5 MeV. These data are continuously multiplexed over individual telescopes with a cadence and resolution of 0.160 s. The 15 SOPA telescopes on the five satellites point in different directions, and the phase of the sampling time varies from satellite to satellite, providing diversity in observing conditions that allows an estimate of systematic errors by comparing measurements across instruments.

The SOPA data for each well-placed detector were deadtime-corrected (with typical deadtimes of $\sim 50\%$) and fit to a spectral form consisting of a power law with an exponential cutoff (a form commonly used to fit gamma-ray burst and SGR spectra). For some of the detectors, the intense portion of the burst was split between two 160 ms time bins, in others the burst was almost entirely contained in a single time bin. This implies that the brightest part of the main spike was less than, but comparable to, 160 ms.

The derived spectra from the spike have 'temperature' parameters (determining the exponential cutoff energy) of $kT \sim 500$ keV with a spread among instruments of $\sim$100 keV, and power-law index parameters of -0.2 with a spread of 0.3. The exponential cutoff is well below SOPA's upper energy limit. An example of such a fit is shown in Supplementary Figure 3. The 1-timebin or 2-timebin integrated fluxes for each SOPA instrument gives $5\,\mathrm{erg\,cm^{-2}\,s^{-1}} \times 0.160 s$, or a fluence of $0.8\,\mathrm{erg\,cm^{-2}}$ above 45 keV. The spread on the derived

fluence parameter across SOPAs is $0.05\,\mathrm{erg\,cm^{-2}}$, which we take as a measure of the systematic uncertainty. (The statistical uncertainty is miniscule compared to the systematics.)

This flux is much higher than our experience with the previous two giant SGR flares. For perspective, the light from the full moon has an energy flux of $3\,\mathrm{erg\,cm^{-2}\,s^{-1}}$. Therefore, verification from other instruments is desired to add to the measurement's credibility.

The Energy Spectrometer for Particles (ESP[s2]) is a higher-energy-range instrument on the same five satellites as SOPA (a pair of ESPs flies on each satellite). Each is a scintillator-photomultiplier combination, with the scintillator being a 3.81 cm dia. × 3.81 cm bismuth germanate cylinder completely surrounded by 0.63-cm thick plastic scintillator as a phoswich. The operation of this instrument includes the measurement of the anode current, sampled every 128 ms (but with an effective integration time of a few ms). These anode currents have been calibrated on the ground by exposure to a ^{60}Co γ-ray source at flux levels up to $360\,\mathrm{erg\,cm^{-2}\,s^{-1}}$. The highest anode currents currents measured during the superflare correspond to a peak flux of 6 $\mathrm{erg\,cm^{-2}\,s^{-1}}$, and so are consistent with the SOPA measurements.

Preliminary results reported[s3] for the RHESSI telescope give lower limits on the fluence $> 0.3\,\mathrm{erg\,cm^{-2}\,s^{-1}}$ over a 3 keV-15 MeV energy range, and $> 0.1\,\mathrm{erg\,cm^{-2}\,s^{-1}}$ above 65 keV. These lower limits are consistent with our (somewhat higher) measurements.

BAT tail fluence determination

The Burst Alert Telescope (BAT)[s4] on *Swift* is a wide (1.5 sr) field of view (FOV) coded aperture telescope designed to rapidly identify and locate Gamma Ray Bursts (GRBs). The detector array is composed of 32768 individual $4 \times 4 \times 2$ mm^3 CdZnTe crystals, each with its own ampifier-discriminator chain, yielding a 5200 cm^2 position-sensitive detector plane with 4 mm resolution and a nominal 15-350 keV energy range.

As *Swift* was oriented at the time of the main spike, the SGR illuminated the detector at an angle of 105° from the center of the field of view. At this angle, the γ-rays passed through or were scattered by the body of the spacecraft, the tube of either the X-Ray Telescope (XRT) or UV and Optical Telescope UVOT (depending on detector location) and a graded-Z shield behind the detector plane. After the first and second slew, giving angles of 61° and 67°, respectively, the γ-rays no longer had to pass through the spacecraft body (although they

still encountered the XRT or UVOT and graded-Z shielding on the sides of the BAT before reaching the detector).

Using an instrumental and spacecraft mass model and Monte Carlo methods, we generated Detector Response Matrices (DRMs) for the 105° and 67° orientations, allowing us to use the XSPEC package to derive fluxes and spectra from count rates. The effective area of the instrument in the 105° orientation is a few hundred cm^2 at photon energies above 100 keV, dropping to $\sim$10 cm^2 around 60 keV and insignificant below 45 keV. In the 67° orientation the effective area was roughly twice that for 105° at photon energies of 60 keV and above, and maintained a small but appreciable effective area of 3 cm^2 at our 15 keV threshold. (In that orientation, low energy photons could pass through the coded aperture mask and scatter off the innermost (copper) layer of the shield directly into the detector.) Strong instrumental fluorescence lines are predicted by the Monte Carlo, and are indeed the most obvious features of the measured spectrum throughout the tail emission.

One of the data products that BAT generates in response to a GRB or other transient is a listing of every detected photon, including the measured energy deposition and the time to 100μs resolution. For transients that are not located (*e.g.*, as in the case of the SGR, when they are not in the BAT's imaged field-of-view), 20 seconds of such data is returned. This is sufficient to produce the high time resolution plot of Figure 1b, but did not include most of the tail emission. However, continuous data is available as count rates in 4 energy bins at 64 ms resolution.

We integrated the count rates in the two highest energy bins (50–100 and 100–350 keV deposited energy) to get the background-subtracted two-channel 'spectra' in three time intervals: before, during, and after the first slew.

These spectra were then fit with XSPEC using two spectral forms: an unbroken power-law (PL) and an Optically Thin Thermal Bremsstrahlung (OTTB). The first interval was fit using the 105° DRM, the third interval was fit using the 67° DRM, and the second interval, the slew, was fit using both. As each individual fit is constrained (two free parameters fitting two spectral bins), and because systematic uncertainties are large while uncertainties

in counting statistics are practically non-existent, χ^2 fit quality is inapplicable and error estimates must come from arguments such as consistency levels among fits.

The PL fits gave large spectral indices $(-5 - -7)$, which is usually an indicator that an exponential cut-off is required by the fit. The OTTB (a spectral form that includes an exponential cut-off) gave fits with temperature parameters in the 15-35 keV range, consistent with previous measurements of giant flare tails. The fit temperature is unreliable, based solely on the 'color' (two-bin count ratio) at energies well above the peak, but the consistency gives qualitative support to the use of this spectral form.

The calculated energy fluxes based on these two spectral forms were consistent within 20% over 60–350 keV. Fits made over the slew interval with the two DRMs varied in calculated fluence by a factor of 2, consistent with the change in effective area over this time interval. Integrating the fluences over all three intervals (using the average fluxes of the two DRMs during the slew interval) gave 0.93×10^{-3} and 1.1×10^{-3} erg cm^{-2} for the OTTB and PL, respectively.

Based on the obvious systematic uncertainties in this procedure, we adopted a systematic error estimate of 50%. This is much larger than the discrepancy between the two models' fits, but many of the systematics of fitting two-parameter models with two measurements are correlated.

In addition, the width of the pulses in each cycle are narrow, indicating that the tail emission is substantially beamed. Measurements at Earth show 3 or 4 peaks, but observers at other latitudes relative to the neutron star would see a different pulse pattern, with a different overall intensity. (*E.g.*, the August 27 1998 tail from SGR 1900+14 showed 4 main peaks with 8 distinct maxima per cycle.) Thus, even perfect measurements would provide limited advantage in determining the total energy radiated during the tail.

Averaging the fluences derived from the two spectral forms yielded our stated fluence of $1.0(5) \times 10^{-3}$ erg cm^{-2}.

BAT deadtime correction

BAT's 32,768 individual CdZnTe detectors are grouped into 256 units, called 'sandwiches'. Each sandwich contains 128 detectors feeding an integrated circuit (the XA-1) that contains 128 amplifier-discriminator chains and a demultiplexer. When a detector absorbs a γ-ray, the signal is amplified, then detected by the discriminator, which triggers circuitry to demultiplex that signal to the XA-1 analog output (giving a measure of the deposited energy) and to indicate which detector was struck. While this data is digitized by circuitry associated with the sandwich, further signals from the 128 detectors of that sandwich are ignored. This 'deadtime' has been measured at $t_{dead} = 98(3)\mu s$. Thus the maximum combined rate at which the 256 sandwiches of BAT can detect photons is the saturation rate $R_{sat} = 256/t_{dead} = 2.61(8) \times 10^6 s^{-1}$.

If the BAT is measuring photons at a rate of r_{meas}, then the average sandwich is dead for r_{meas}/R_{sat} of the time, so the detector rate can be deadtime corrected by dividing by the livetime fraction: $r_{corr} = r_{meas}/(1 - r_{meas}/R_{sat})$. As r_{meas} approaches R_{sat} the uncertainty in t_{dead} makes r_{corr} poorly determined. Thus the deadtime correction from BAT measured count rate to photon rate is currently highly uncertain above $r_{corr} \gtrsim 20R_{sat}$. Above $r_{corr} \gtrsim 30R_{sat}$ the formal error range includes infinite flux as the deadtime is consistent with 100%. The peak fluxes from SOPA indicate that the true photon rate on the BAT detector was $\sim 10^3 R_{sat}$, and so even a much more accurate t_{dead} determination would have resulted in a a poor estimate of r_{corr} at the peak. Thus SOPA and ESP are needed to provide the peak measurements that BAT cannot.

---

s1. Belian, R. D., Gisler, G. R., Cayton T., Christensen, R. High-Z energetic particles at geosynchronous orbit during the great solar proton event series of October 1989. *JGR***97(A11))** 16,897–16,906 (1992).

s2. Meier, M. M., Belian, R. D., Cayton, T. E., Christensen, R. A., Garcia, B., Grace, K. M., Ingraham, J. C., Laros, J. G., Reeves, G. D., The Energy Spectrometer for Particles (ESP): instrument description and orbital performance. in the proceedings of *Workshop on the Earth's Trapped Particle Environment*, AIP Conference proceedings **383** 203–210 (1996).

s3. Boggs, S., Hurley, K., Smith, D. M., Lin, R.P., Hurford, G., Hajdas, W., & Wigger, C. SGR 1806-20, RHESSI observations of the 041227 giant flare. *GCN* **2936** (2005).

s4. Barthelmy, S.D. Burst Alert Telescope (BAT) on the Swift MIDEX mission. *SPIE* **5165**, 175–189 (2004).
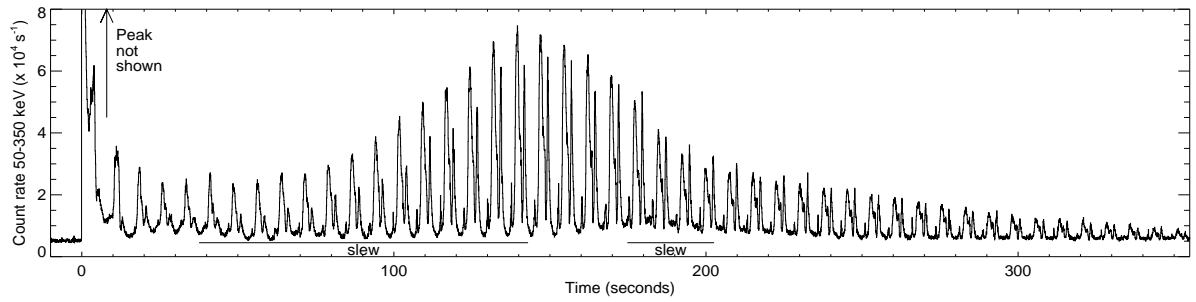
Figure 1a: The SGR spike and tail light curve from the Burst Alert Telescope (BAT) on *Swift* at measured energy $>50\,\mathrm{keV}$ (64 ms bins). Although BAT was pointed $105°$ away from the SGR at the time of the main spike, it recorded $\gamma-$rays above $60\,\mathrm{keV}$ passing through and scattering within the spacecraft body and instrument shielding. As part of a pre-planned observing schedule, *Swift* slewed to observe a different source shortly after the main peak, reaching a steady pointing direction $61°$ from the SGR at 143 seconds. The spacecraft re-orientation improved the detection efficiency of the SGR, visible as an apparent (not intrinsic) rise in the light curve to a peak at 140 s. This is followed by a second slew to $67°$.
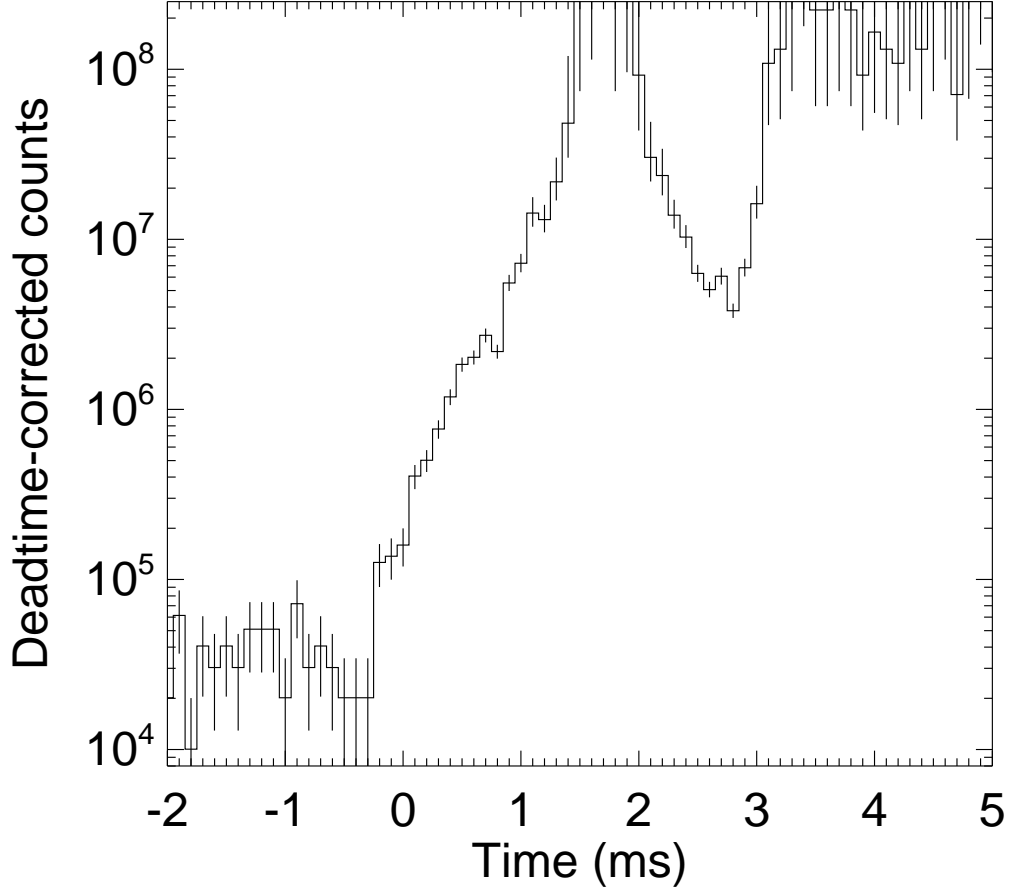
Figure 1b: BAT deadtime-corrected count rate (all energies) during the complex leading edge of the main spike. (Note that horizontal scale is 10^4 larger than *1a*.) Uncertainties in the deadtime correction (discussed in *Supplementary Methods*) make corrected count rates increasingly unreliable above 5×10^7 counts per second. Time bins of $100\mu s$ are equivalent to the light-crossing-time of a neutron star diameter. More detailed lightcurves are shown in the *supplementary figures* section.
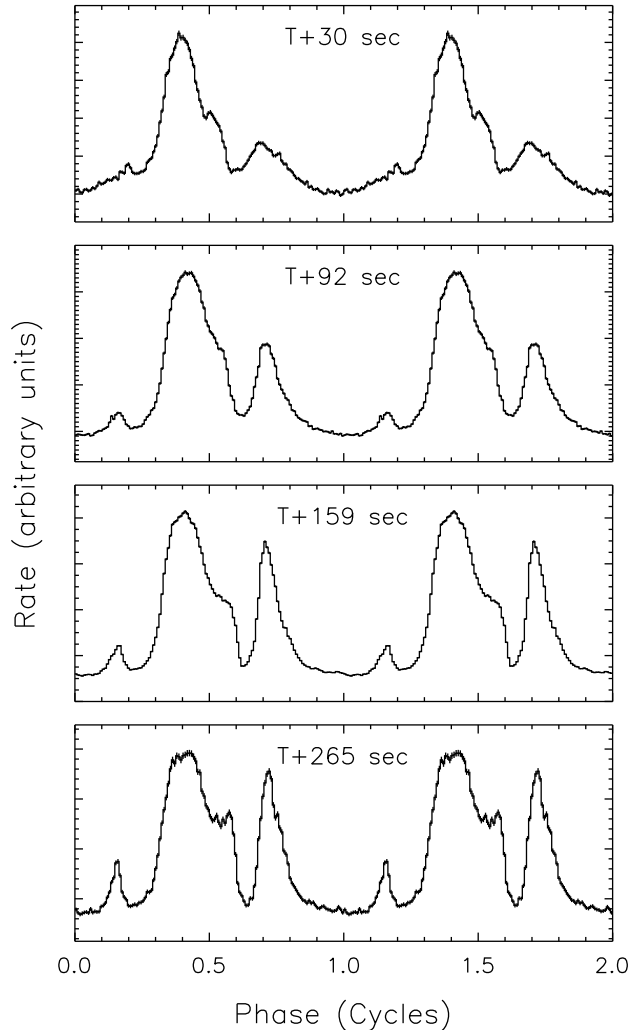
Figure 2: The pulse profile evolution of the magnetar SGR 1806–20 during the giant flare of 2004 December 27. Time through the flare increases from top to bottom. Each panel displays the pulse profile folded over four pulse cycles at one of four different time intervals during the flare. The times denoted at the top of each panel indicate the midpoint of the interval relative to the onset of the flare. During the first half of the tail (∼170 s), the peak centered at phase 0.7 grows in amplitude as the primary peak fades until the two are nearly equal in height. Thereafter, the two peaks decay in lockstep while the relative amplitude of the third peak at phase 0.2 increases. Overall, the pulse profile becomes less sinusoidal during the course of the flare, that is, the power in the higher harmonics increases relative to the power at the fundamental frequency, opposite to what was seen in SGR 1900+14 during the August 27 flare.[24] The phases of the SGR 1806–20 pulse peaks remain fixed, indicating a finalized magnetic geometry, and supporting the notion that after the first spike no new magnetic energy is released, and only the trapped fireball energy leaks out. The individual pulses throughout the tail can be seen in *Supplementary figure* 1.
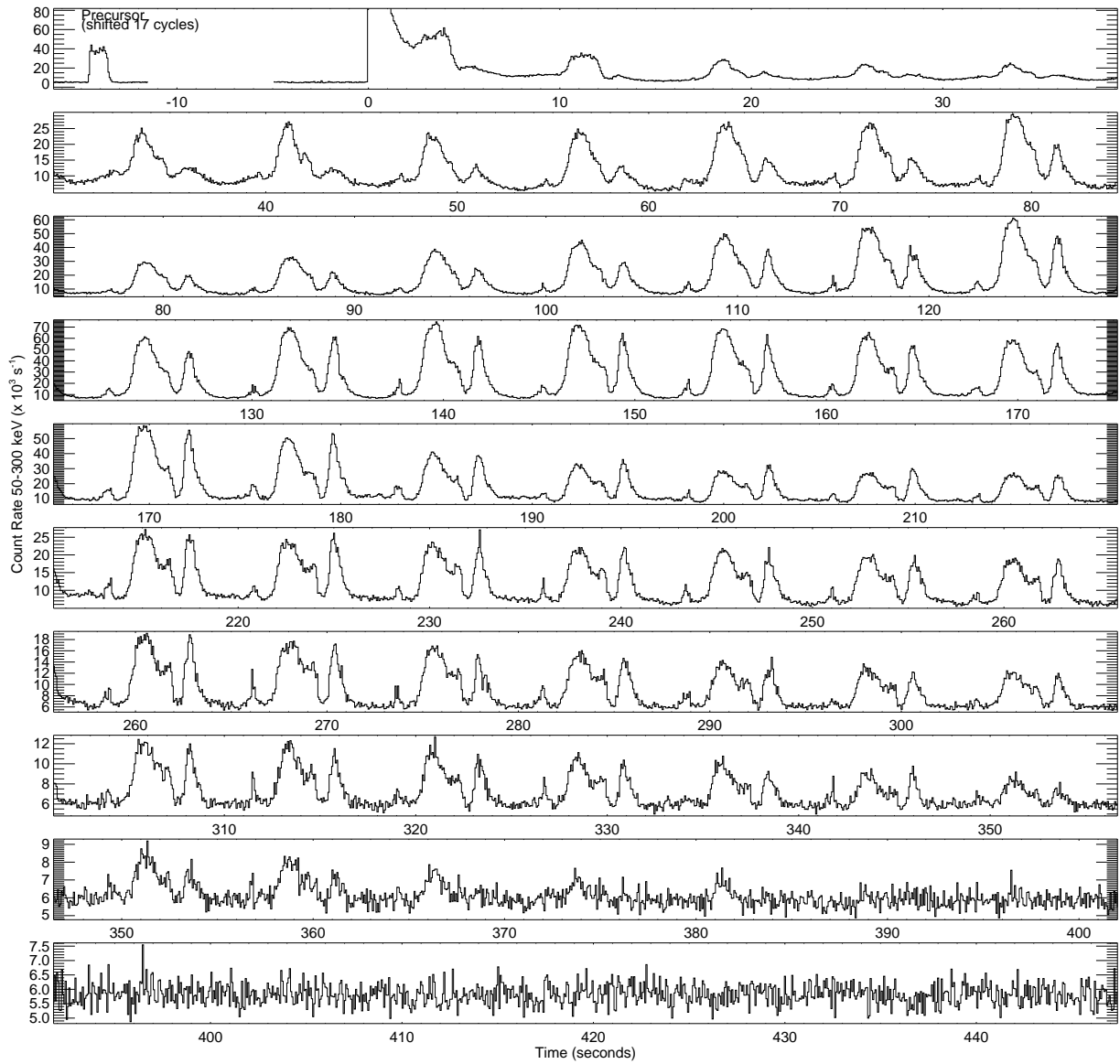
Supplementary Figure 1: BAT lightcurve of the precursor and tail of the giant flare with 64 ms resolution. Successive plots are phase aligned at the 7.56 s neutron star spin frequency, with one cycle of overlap from plot to plot. The precursor, which occurred 142 s before the spike, is plotted at the appropriate spin phase.
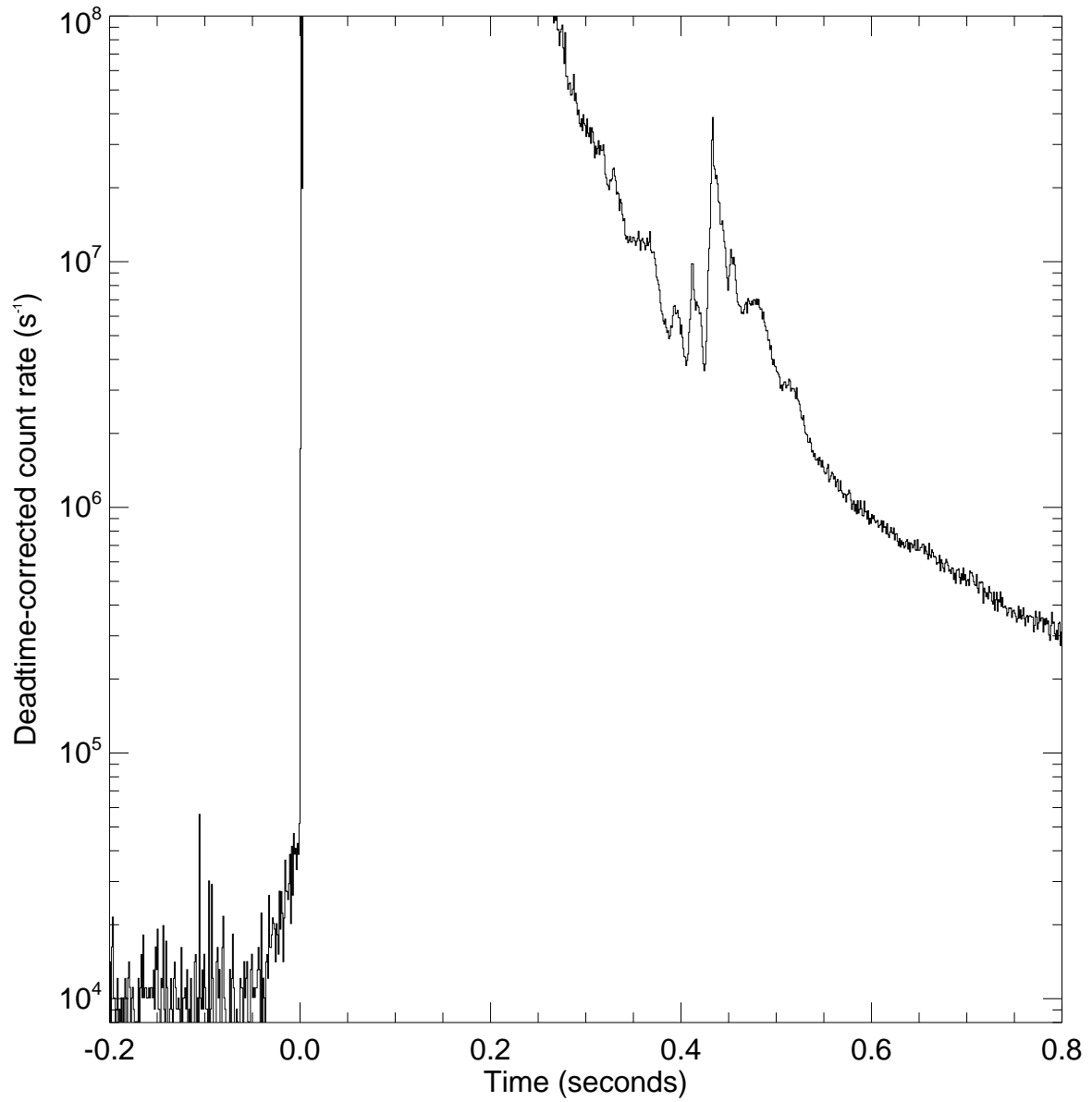
Supplementary Figure 2: BAT deadtime-corrected lightcurve leading up to and during the decline of the main spike, with 1 ms resolution. Corrected rates above 5×10^7 have large uncertainties in the deadtime correction.
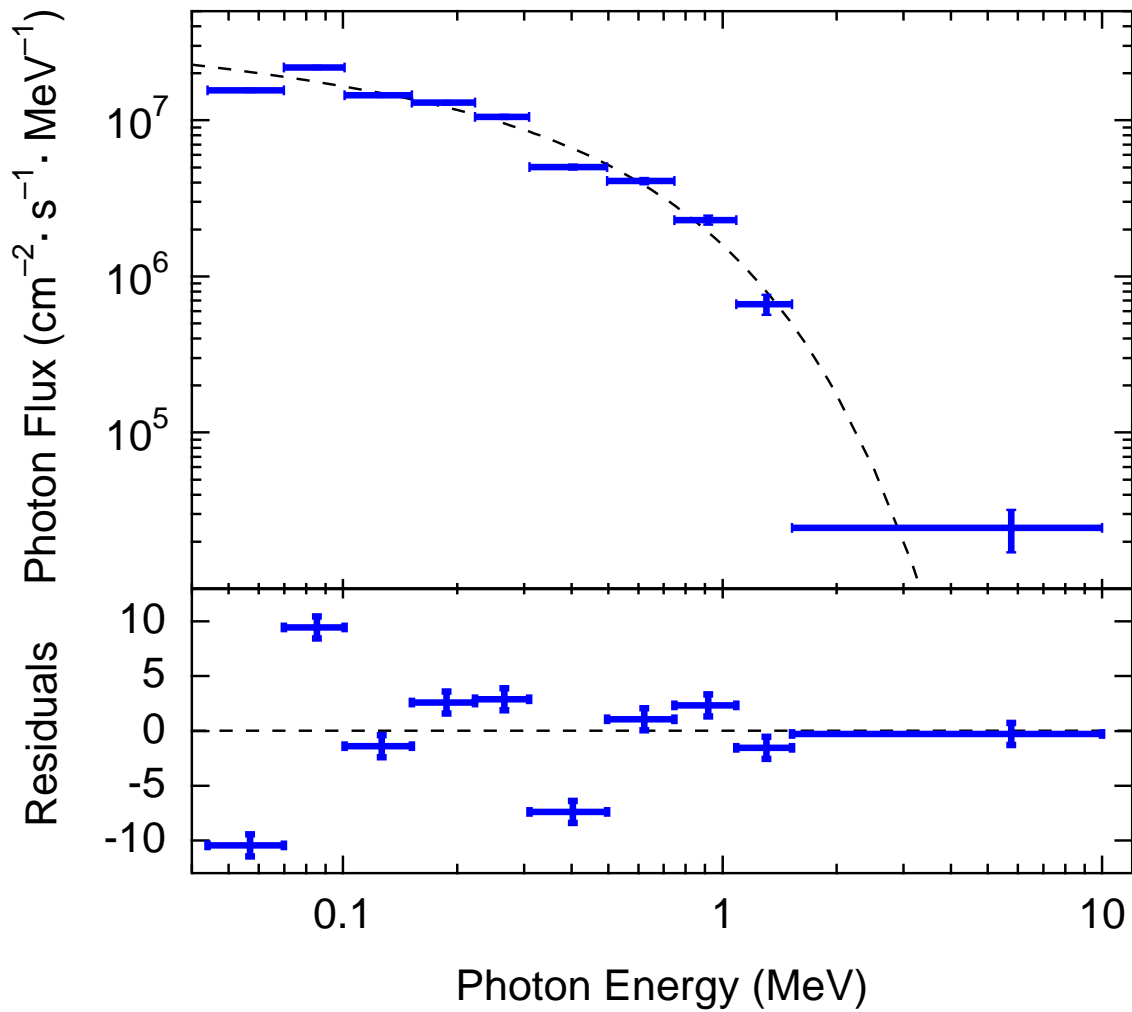
Supplementary Figure 3: A spectral fit to SOPA data. This is an example of a spectral fit to data from one of the SOPA detectors to the peak 0.160 s of the main spike. The dashed line is the spectral model in photons, with a low energy power law α= -0.2 and an exponential cut-off kT = 0.48 MeV.